

***g*-factor and well-width fluctuations as a function of carrier density in the two-dimensional hole accumulation layer of transfer-doped diamond**

Golrokh Akhgar,^{1,*} Lothar Ley,^{1,2} Daniel L. Creedon,³ Alastair Stacey,³
Jeffrey C. McCallum,³ Alex R. Hamilton,⁴ and Christopher I. Pakes^{1,†}

¹*Department of Chemistry and Physics, La Trobe University, Victoria 3086, Australia*

²*Institute of Condensed Matter Physics, Universität Erlangen, Staudt-Str. 1, 91058 Erlangen, Germany*

³*School of Physics, The University of Melbourne, Victoria 3010, Australia*

⁴*School of Physics, University of New South Wales, Sydney, New South Wales 2052, Australia*



(Received 9 October 2018; revised manuscript received 11 January 2019; published 29 January 2019)

The two-dimensional (2D) hole gas at the surface of transfer-doped diamond shows quantum-mechanical interference effects in magnetoresistance in the form of weak localization and weak antilocalization (WAL) at temperatures below about 5 K. Here we use the quenching of the WAL by an additional magnetic field applied parallel to the 2D plane to extract the magnitude of the in-plane *g*-factor of the holes and fluctuations in the well width as a function of carrier density. Carrier densities are varied between 1.71 and $4.35 \times 10^{13} \text{ cm}^{-2}$ by gating a Hall bar device with an ionic liquid. Over this range, calculated values of $|g|$ vary between 1.6 and 2.3 and the extracted well-width variation drops from 3 to 1.3 nm rms over the phase coherence length of 33 nm for a fixed geometrical surface roughness of about 1 nm as measured by atomic force microscopy. Possible mechanisms for the extracted variations in the presence of the ionic liquid are discussed.

DOI: [10.1103/PhysRevB.99.035159](https://doi.org/10.1103/PhysRevB.99.035159)

I. INTRODUCTION

Undoped diamond is a bona fide insulator. However, when the surface is terminated with hydrogen and exposed to air it develops a pronounced *p*-type surface conductivity through a process that is termed transfer doping [1]. Transfer doping involves an electrochemical reaction between diamond and the ever-present water layer that leaves holes in the diamond valence bands and compensating OH^- ions at the surface [2]. As space charges, the holes are confined by a strong upward band bending to a narrow two-dimensional (2D) well right below the surface. Typical carrier concentrations are 10^{12} to 10^{13} cm^{-2} and the width of the well depends self-consistently on carrier density and lies in the range of 1 to 10 nm [3]. Because transfer doping does not involve the activation of an acceptor there is no carrier freeze-out and metallic conductivity is maintained down to at least 250 mK. Low-temperature magnetoresistance measurements show that electrical transport in the hole accumulation layer exhibits quantum phenomena that are characteristic for a 2D quantum system and lead to a deviation from classical Drude conductivity. They are Shubnikov–de Haas oscillations [4], a strong hole-hole interaction (HHI), quantum interference effects that show up as weak localization (WL) [5], and weak antilocalization (WAL) due to strong spin-orbit interaction [5]. Using an ionic liquid (IL) as a gate dielectric we were able to increase the carrier density from 1.1 to $7.23 \times 10^{13} \text{ cm}^{-2}$ with a proportional increase in spin-orbit splitting from 4.6 to 24.5 meV [6]. This large spin-orbit splitting observed for

a 2D hole system exceeds the atomic spin-orbit splitting of the valence electrons in diamond ($\Delta_{\text{atomic}} = 8 \text{ meV}$) [7]. Because the electric field in the highly asymmetrical confining potential increases with carrier density, the enhanced spin-orbit splitting was ascribed to the Rashba effect. In particular, here it is ascribed to the Rashba effect cubic in wave-vector *k* for reasons explained in Ref. [8].

With a strong spin-orbit interaction the holes in diamond are potential candidates for spin manipulation. While the Rashba effect provides the coupling of the carrier spin to an electric field, the strength of the coupling to a magnetic field, i.e., the carrier *g*-factor, was still missing. That gap was recently closed by us following Minkov *et al.* [9] and measuring the low-temperature magnetoresistance as a function of a magnetic field perpendicular to the 2D hole gas with an additional parallel field as a parameter [10]. The analysis of the data yields for the magnitude of the *g*-factor a value of 2.6 ± 0.1 . In addition, the data showed additional effects due to variations in effective well width of 3-nm mean-square roughness over a distance of about 30 nm [10].

Here we extend these measurements to hole concentrations that are tuned by an ionic liquid gate over the range from 1.71 to $4.35 \times 10^{13} \text{ cm}^{-2}$. The analysis gives a monotonically rising *g*-factor while the effective well-width variation decreases with increasing carrier concentration. Mechanisms are discussed to rationalize these observations.

II. EXPERIMENT

A commercial IIA single-crystal (001) diamond face was used to fabricate the Hall bar device. The surface was hydrogen terminated at approximately 850 °C in a microwave hydrogen plasma with a power of 1500 W for 10 min. In order to

*g.akhgar@latrobe.edu.au

†c.pakes@latrobe.edu.au

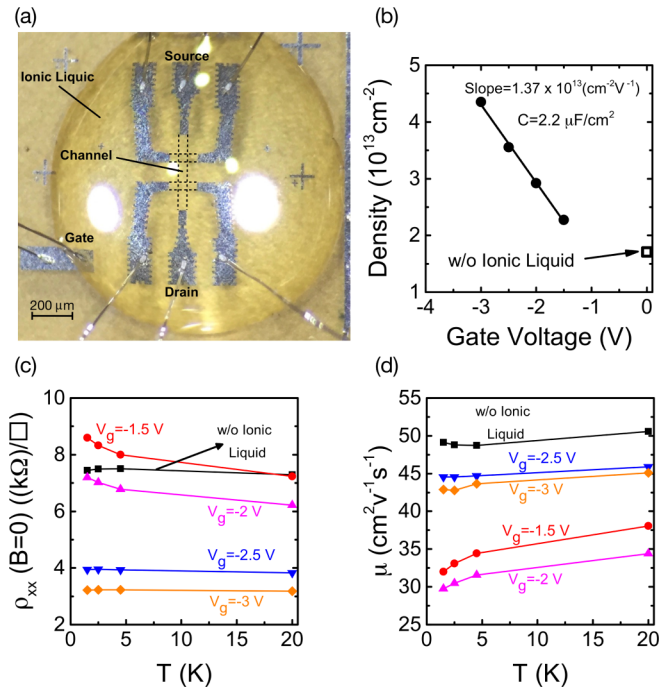


FIG. 1. (a) Optical image of the ionic liquid gated Hall bar device. The two bright spots are reflections of the overhead light on the surface of the ionic liquid. (b) Hole sheet density as a function of gate voltage. (c), (d) Hole sheet resistivity and mobility, respectively, as a function of temperature with gate voltage as parameter.

achieve saturation charge-transfer doping, the sample was left in air for several days following the termination. A Hall bar with channel length and width of 200 and 40 μm , respectively, and palladium contacts was fabricated using standard photolithography and lift-off processing. The conducting regions are isolated from the rest of the surface by oxygen plasma exposure. The Hall bar device was gated using the ionic liquid 1-ethyl-3-methyl-imidazolium tris(pentafluoroethyl) trifluorophosphate $[\text{C}_2\text{C}_1\text{Im}]^+[\text{FAP}]^-$ as a high-capacity gate insulator. The IL is dropped on the channel of the device using a micropipette, ensuring coverage on the gate contact as well [Fig. 1(a)]. The gate bias is applied above the IL melting point of 236 K in order to ensure the full IL polarization. After cooling below the melting point the polarization is maintained and potentials on any of the contacts have no influence on the effective gate voltage. Magnetotransport measurements are performed using a Leiden Cryogenics dry dilution refrigerator with an integrated 9-1-1 T superconducting vector magnet. Longitudinal and Hall resistivity are measured at temperatures from 1.5 to 20 K for perpendicular magnetic fields B_{\perp} up to 1 T and gate biases between 0 and -3.0 V. Zeeman splitting and microroughness for each gate voltage are derived from magnetoresistance measurements at 2.5 K when in addition to B_{\perp} a constant in-plane field B_{\parallel} between 0 and 1 T is applied in steps of 0.2 T.

III. RESULTS

The analysis of the data follows the one used in our previous publications [5,6,10]. As a first step, HHI is removed

from ρ_{xx} and ρ_{xy} by applying a correction to the measured data according to Goh *et al.* [11] and the procedure is explained in the Supplemental Material [12]. From these corrected data the longitudinal conductivity σ_{xx} , carrier concentration, and mobility, all as a function of gate voltage, are derived in the usual way. The sample exhibits metallic conductivity down to the lowest temperatures except for gate voltages of -1.5 and -2.0 V, where a slight increase in longitudinal sheet resistivity is observed [Fig. 1(c)]. For these two gate voltages the mobilities are noticeably lower than for the remainder of the gate voltages [Fig. 1(d)] where mobilities are within the range reported consistently for air-induced surface conductivity [13,14]. Since mobility and longitudinal resistivity are back to normal at -3.0 -V gate voltage there is no apparent deterioration in sample properties with increasing gate voltage, and no peculiar behavior in magnetoresistance has been detected either. As intended, the carrier concentration increases linearly with gate voltage albeit with a slightly smaller slope compared to our earlier work as reflected in the ionic liquid capacitance of $2.2 \mu\text{F}/\text{cm}^2$ vs the previous $2.8 \mu\text{F}/\text{cm}^2$ [6]. Other salient quantities such as diffusion constant, elastic-scattering times, and mean-free path are collected in the Supplemental Material [12].

We turn now to the magnetoconductance data without application of a field component parallel to the 2D plane (see the σ_{xx} vs B curves for $B_{\parallel} = 0$ in Fig. 2). For the lowest carrier density without ionic liquid the magnetoconductivity exhibits the drop in σ_{xx} around $B_{\perp} = 0$ characteristic of weak localization that is modified by the central, cusplike peak due to weak antilocalization. The WAL feature increases with gate voltage and thus carrier concentration until it is the dominant feature of the magnetoconductivity starting at $V_g = -2.0$ V.

WAL is due to spin-orbit interaction which destroys the constructive interference necessary for WL. Spin-orbit interaction can ultimately even lead to a conductivity that exceeds the Drude conductivity due to the destructive interference of time-reversed backscattering loops [15]. WL is partly restored by coupling the spins to the external magnetic field which accounts for the cusplike appearance of WAL in the spectra. The magnetoconductance curves are fitted to the expression derived by Hikami *et al.* [16] as given by Knap *et al.* [17] for k^3 Rashba spin-orbit interaction. From the fits, crucial parameters such as the phase and spin coherence lengths of the carriers and their spin-orbit splitting Δ_{so} are derived. These quantities are collected in the Supplemental Material [12] and Δ_{so} exhibits a linear increase with carrier density reported previously [6]. The increase is characteristic for spin-orbit interaction due to the Rashba effect because there is a direct connection between carrier density and electric-field strength in the carrier confining quantum well on account of Gauss's law: higher carrier densities result in more asymmetric quantum wells.

Turning to the traces with parallel field component we observe a quenching of the WAL feature with increasing B_{\parallel} . This is most apparent for the lowest carrier densities where WAL is still rather weak in the absence of B_{\parallel} . Two factors contribute to this reduction: fluctuations in effective well width and the Zeeman effect [18,19]. They are accounted for in the Hikami formula for the change in conductance $\Delta\sigma$ by

two additional parameters Δ_r and Δ_s [9]:

$$\Delta\sigma = \frac{e^2}{2\pi^2\hbar} \left[\begin{array}{l} \Psi\left(\frac{1}{2} + \frac{B_\phi + B_{so} + \Delta_r}{B_\perp}\right) + \frac{1}{2}\Psi\left(\frac{1}{2} + \frac{B_\phi + 2B_{so} + \Delta_r}{B_\perp}\right) \\ -\frac{1}{2}\Psi\left(\frac{1}{2} + \frac{B_\phi + \Delta_s + \Delta_r}{B_\perp}\right) - \ln\left(\frac{B_\phi + B_{so} + \Delta_r}{B_\perp}\right) - \frac{1}{2}\ln\left(\frac{B_\phi + 2B_{so} + \Delta_r}{B_\perp}\right) \\ +\frac{1}{2}\ln\left(\frac{B_\phi + \Delta_s + \Delta_r}{B_\perp}\right) \end{array} \right]. \quad (1)$$

Here, Ψ is the digamma function and B_ϕ and B_{so} are characteristic fields that scale with the phase-breaking inelastic-scattering rate $1/\tau_\phi$ and the spin-relaxation rate $1/\tau_{so}$ due to spin-orbit interaction according to $1/\tau_\phi = 4eDB_\phi/\hbar$ and $1/\tau_{so} = 4eDB_{so}/\hbar$, where D is the diffusion constant.

Fluctuations in the well width mean carriers that are backscattered and interfere after traversing time-reversed loops are no longer confined strictly to a plane and will therefore be susceptible to a magnetic field parallel to the 2D plane. This allows an additional Aharonov-Bohm phase to be involved. Hence $\Delta_r = \frac{\sqrt{\pi}}{2} \frac{e}{\hbar} \frac{d^2L}{l} B_\perp^2$ is added to B_ϕ in the above formula as an additional phase-breaking effective field that

scales with $\frac{d^2L}{l}$, the product of the mean-square well-width fluctuations d^2 and the correlation length of the fluctuations L divided by l , the elastic mean-free path.

The term $\Delta_s = \frac{\tau_{so}}{4e\hbar D} (g\mu_B B_\parallel)^2$ scales with the square of the in-plane Zeeman splitting $g\mu_B B_\parallel$ where g and μ_B are the g -factor of the carriers and the Bohr magneton, respectively. The correction Δ_s is applied only to the singlet term (dependent on B_ϕ only) and not the triplet term (dependent on B_ϕ and B_{so}) in Eq. (1) [9].

All magnetoconductivity curves for $B_\parallel = 0$ were first fitted to Eq. (1) with Δ_r , Δ_s set to zero. From these fits the characteristic fields B_ϕ and B_{so} are derived which in turn yield the inelastic- and spin-orbit scattering times and the spin-orbit splitting as a function of gate voltage and hence carrier density. All these values are collected in the Supplemental Material and they are in agreement with earlier data derived from the magnetoconductivity of the hole gas in diamond in the absence of B_\parallel [5,6].

Next, Δ_r and Δ_s were varied in Eq. (1) to fit the curves for finite B_\parallel while keeping B_ϕ and B_{so} fixed at the value previously determined for each gate voltage in the absence of B_\parallel . Satisfactory fits were obtained as demonstrated by the solid lines in Fig. 2 for a selection of gate voltages. In Fig. 3, Δ_r and Δ_s so obtained are plotted vs B_\perp^2 . Both scale—the latter with some scatter—linearly with B_\perp^2 as required for Eq. (1) to be applicable. From the slopes of linear regressions, the factors d^2L and g are calculated according to the above expressions and they are plotted as a function of carrier density in Fig. 4.

The error bars were calculated using error progression from the standard deviations obtained in the fitting procedures or estimated as 5% for the diffusion constant D . D is directly traced to the Drude conductivity σ_D and this error therefore reflects the precision of the conductivity measurement. However, we ascribe a considerably larger systematic error of 20% to D that represents the uncertainty in identifying the conductivity at 30 K with the true Drude conductivity at the measurement temperature.

IV. DISCUSSION

The use of magnetoresistance as a nondestructive method to characterize the roughness of 2D systems was pioneered by Wheeler and coworkers [20–22], and it was taken up by Minkov *et al.* [23] and Cabañas *et al.* [24] with the theoretical underpinning provided by Mathur and Baranger [25]. In these works the attenuation of weak localization in the presence of an additional magnetic field parallel to the plane of the 2D system was taken as evidence for interface roughness in Si/SiO₂ interfaces of metal-oxide-semiconductor field-effect transistor (MOSFET) structures [20–22] and of well-width

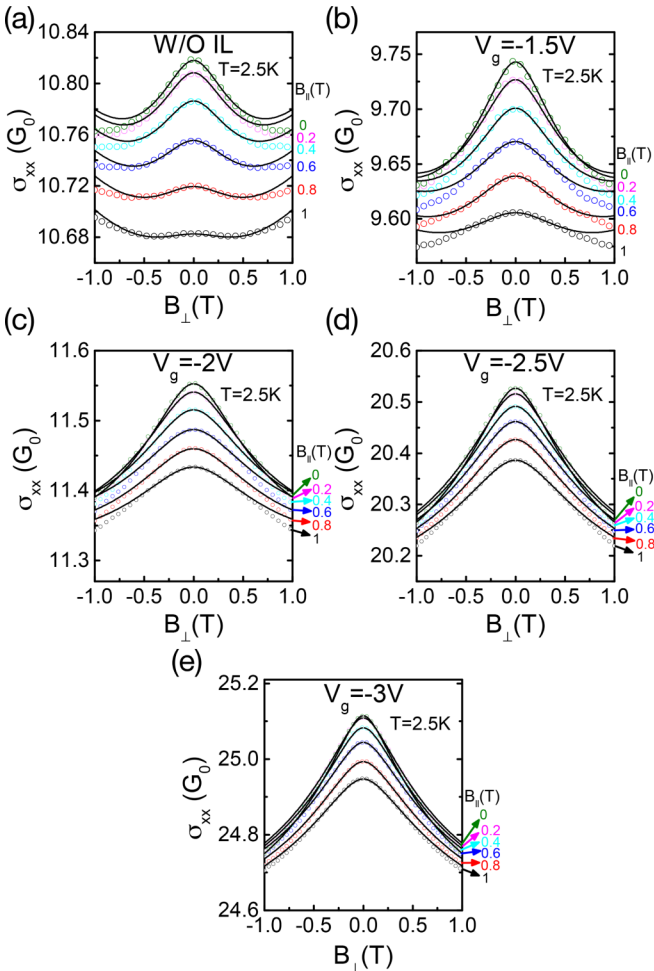


FIG. 2. Longitudinal conductivity σ_{xx} as a function of B_\perp with different applied in-plane fields B_\parallel : (a) when the device is ungated, without ionic liquid; (b)–(e) with gate biases of -1.5 , -2 , -2.5 , and -3 V, respectively. The open circles are the data points and the lines are the fits.

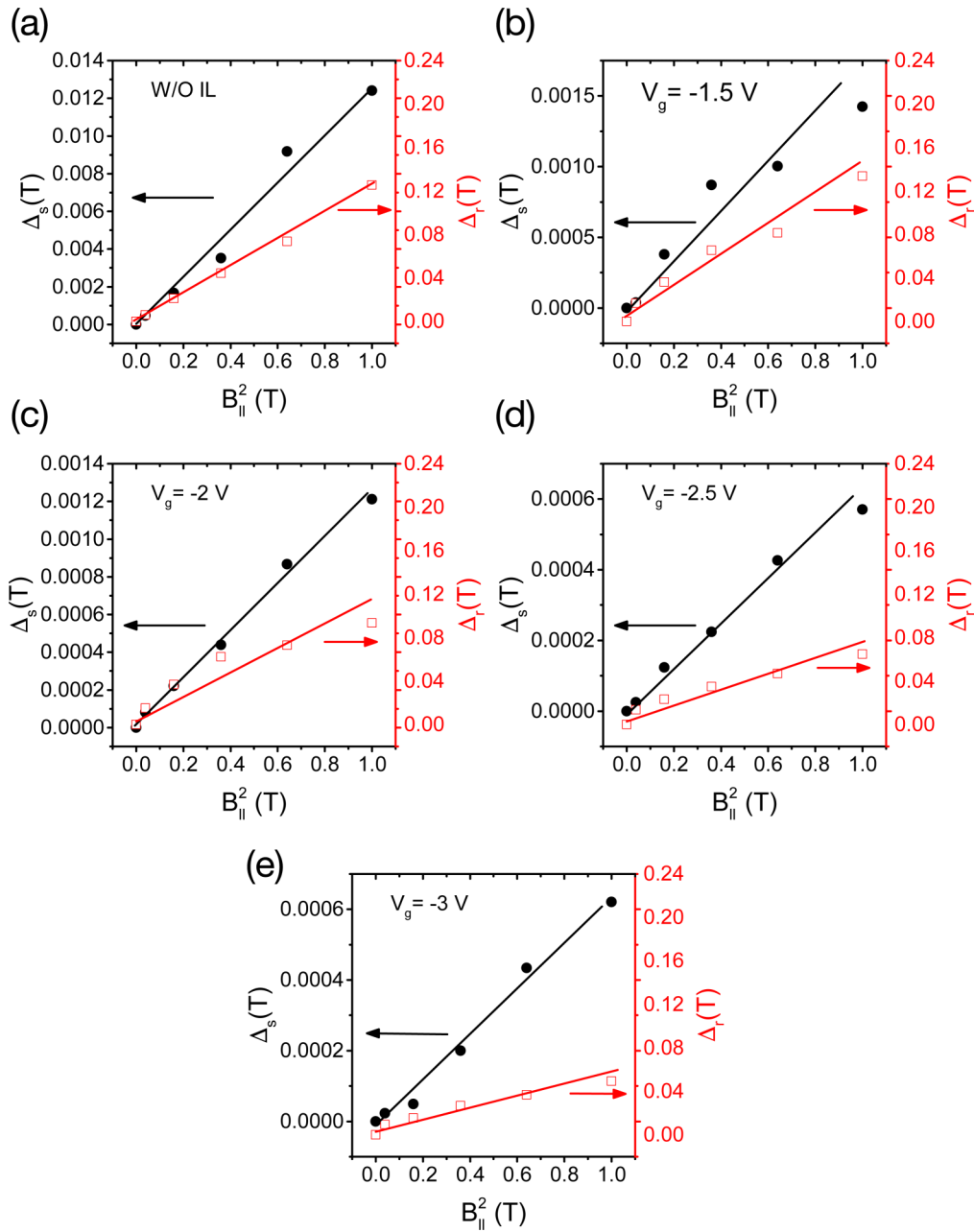


FIG. 3. Parameters Δ_s and Δ_r as extracted from fits to the magnetoconductivity curves in Fig. 2 plotted vs $B_{||}^2$ for the gate voltages indicated in each frame; W/O IL: without ionic liquid. The lines are linear regressions to the data points.

fluctuations in an AlGaAs heterostructure [20]. In all cases the interpretation follows the one given here, namely the addition of a $B_{||}$ -dependent phase-breaking rate when the time-reversed electron loops deviate from a strictly planar path and thus expose open loops to $B_{||}$ as well. Interface roughness or well-width variations are extracted analogously to the procedure described above, and qualitative [22] as well as quantitative [23] agreement between the interface roughness determined by magnetoresistance and atomic force microscopy has been reported. In one case, the interface roughness parameter was determined as a function of carrier density in the inversion channel of a gated MOSFET device [21]. Here, despite an unchanged topological roughness, the apparent magnetoresistance roughness increased about twofold for an increase in

carrier density by a factor of three. The authors ascribe that to the fact that the electron wave function is brought closer to the interface as the confining potential narrows with increasing carrier density and hence becomes more susceptible to the interface roughness. This is the opposite of what we observe and we shall come back to it below.

The first to study the effect of interface roughness and Zeeman splitting on weak antilocalization in the presence of a parallel field component were Minkov *et al.* [9] and they derived g -factor and interface roughness for carriers in an InGaAs quantum well. Similar work on the 2D electron gas induced by the intrinsic polarization of GaN at the AlGaAs/GaN interface was performed by Cabañas *et al.* [24], for example. However, this is an instance where both interface roughness or

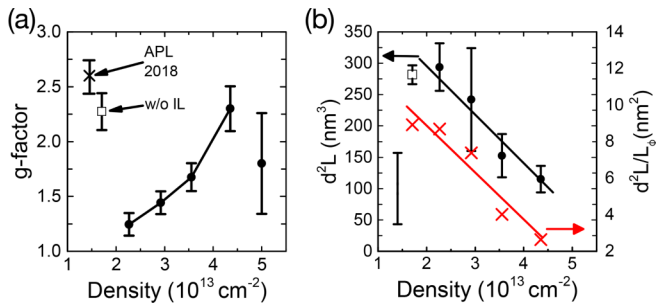


FIG. 4. (a) In-plane g -factor and (b) microroughness parameters d^2L as calculated from the slopes of the lines in Fig. 3 vs hole density. The error bars on each data point are the statistical errors. An overall 20% systematic error due to the uncertainty in the diffusion constant (see text) is indicated by the isolated error bar. The solid lines are guides to the eye and APL 2018 refers to the g -factor of Ref. [10].

well-width variation and in-plane g -factor are systematically studied as a function of carrier density in a 2D hole gas.

We start with the result for the in-plane g -factor as given in Fig. 4(a). We tacitly presuppose that we are always talking about the magnitude of the g -factor in what follows and ignore for the time being the 20% systematic uncertainty alluded to above. It is satisfying albeit to be expected that the g -factor without IL agrees with that derived previously for an ungated device of otherwise identical properties [10]. Once the IL is in place the calculated in-plane g -factor increases monotonically from 1.3 to 2.3 as the carrier density is doubled from 2.2 to $4.4 \times 10^{13} \text{ cm}^{-2}$, thus bracketing the free-electron value of $g = 2$. Similar values were previously derived by the same method for electrons in the InGaAs quantum well (1.7 ± 0.3) [9], and 1.95 in an AlGaAs/GaN interface layer [24]. In lieu of any relevant measurements or calculations of the g -factor for the valence bands of diamond we can only speculate about the origin of the variation in g -factor. Since any deviation from $g = 2$ has to be a band-structure effect, two closely related factors come to mind: band filling and hybridization. As shown previously [3], the carriers in the hole accumulation layer of diamond occupy the lowest 2D band based on the first quantum state derived from the heavy-hole valence band in bulk diamond. The next higher, empty band is that based on the lowest quantum state derived from the light-hole valence band. These two bands eventually cross for sufficiently large k vectors because the “light-hole band” has an effective mass that is larger than the 2D mass of the “heavy-hole band” for in-plane dispersion. Hence, any filling of the heavy-hole band moves the Fermi wave vector k_F closer to the crossing point and thus increases the hybridization of the states that matter for transport. A change in hybridization of the two bands as a consequence of varying carrier densities could give rise to changes in g -factor. However, there is a caveat. As the carrier density increases, the width of the confining potential decreases, which in turn affects the quantization energies of the heavy- and light-hole bands, i.e., their energy at $k = 0$. That could, in principle, overcompensate the band-filling effect and move the energies of the two bands at k_F apart.

Using a simple band calculation, based upon a triangular well approximation [26], the 2D hole dispersion of the light-hole and heavy-hole bands has been estimated, as shown in the

Supplemental Material [12]. For the carrier densities achieved in this experiment, the Fermi wave vector is predicted to reside well below the crossing point so the extent of hybridization of the two bands may be limited. However, the exact mechanism has to await a full calculation including the self-consistent solution of the Schrödinger and Poisson equations along the lines given in Ref. [3].

We now turn to the roughness parameter d^2L as shown as a function of carrier density by the full circles in Fig. 4(b). Again, our present result for the ungated device (open square) agrees with that of our previous publication (280 nm^3) [10]. Because well-width fluctuations beyond the scale of the phase-coherence length L_ϕ are of no relevance to the analysis presented here, we show by the red crosses in Fig. 4(b) the roughness parameter divided by L_ϕ . This should represent directly an effective mean-square roughness and it is clear from its carrier dependence that geometrical surface roughness alone cannot explain our results because the latter would not depend on carrier density. Indeed, in Ref. [10] we reported—measured by atomic force microscopy (AFM)—a mean-square surface roughness of $d_{\text{AFM}}^2 = 1.2 \pm 0.3 \text{ nm}^2$ over a correlation length on the order of the phase-coherence length L_ϕ of about 30 nm. Significantly, this is the value that our current data approach from above as the carrier density increases. Hence it is obvious that the bulk of the measured roughness is due to fluctuations in well width rather than surface roughness. For the ungated device a fluctuation in well width of about 3 nm would be required to obtain the measured d^2 of about 10 nm^2 provided the two contributions, surface roughness and well-width fluctuations, are uncorrelated and add geometrically. Well-width fluctuations of about 3 nm could arise from lateral variations in carrier density by about one order of magnitude [3]. This is in keeping with the requirement of spatially inhomogeneous carrier densities of a comparative level in order to interpret Shubnikov-de Haas oscillations in the hole accumulation layer on (111) diamond [4]. The reduction in well-width fluctuation would then be the result of a more homogeneous carrier distribution as more holes are attracted to the 2D layer with increasing gate voltage.

Lateral inhomogeneities in carrier density may be traced to the haphazard transfer-doping mechanism with its statistical distribution of OH^- anions in the adsorbed water layer. We note that the above analysis does not consider the possibility that the introduction of the ionic liquid layer may modify the correlation length and magnitude of these doping fluctuations in a manner which would affect the applicability of Eq. (1). In Fig. 3, a linear fit was used to describe the dependence of the correction Δ_r on B_{\parallel}^2 , consistent with Eq. (1). However, for cases where the IL is in place, the experimental data may exhibit a nonlinear line shape. Additionally, we presently have no explanation for the substantial drop in g -factor as the IL is placed on the device despite the very small change in carrier density. The above analysis considers only well-width fluctuations that are short range, where $L \sim l$, which introduce an additional dephasing on the WAL but do not affect the line shape of the corresponding magnetoconductance curves. It is possible that the introduction of the IL may modify the distribution of OH^- anions, for example due to the distortion that may arise in the IL as it is cooled, causing deviations in

the short-range fluctuations. The introduction of long-range correlations in the doping distribution would give rise to changes in the line shape of the WAL magnetoconductance curves in a way that would modify the analysis presented here. The correlation length of doping fluctuations in the IL requires a more detailed investigation but this mechanism may illuminate the differing behavior of the data obtained with and without the IL in place.

V. SUMMARY

We have presented here a systematic investigation of g -factor and well-width fluctuations in the hole accumulation layer of diamond as a function of carrier density. The results were obtained by analyzing the quenching of the weak antilocalization feature in the low-temperature magnetoresistance as a function of a magnetic-field component parallel to the 2D hole gas while the carrier density was varied by an ionic liquid gate. For carrier densities between 2.27 and $4.35 \times 10^{13} \text{ cm}^{-2}$ the magnitude of the in-plane g -factor increases

monotonically from 1.3 to 2.3 . The roughness parameter derived from the same measurements drops by a factor of three over the same range of densities and it is evident that initially the geometrical surface roughness as measured by atomic force microscopy contributes only marginally. The main contribution comes from variations in well width traced to lateral inhomogeneities in carrier density. The carrier inhomogeneity is smoothed out as more holes are pulled in by the gate voltage and the roughness parameter approaches within a factor of two the geometrical surface roughness. Variation of the correlation length of fluctuations in the doping distribution in the presence of an ionic liquid, and indeed other commonly used adlayer materials such as transition-metal oxides or gate dielectrics, are likely to influence the spin transport properties in the underlying hole gas.

ACKNOWLEDGMENTS

This work was supported by the Australian Research Council under the Discovery Project No. DP150101673.

-
- [1] C. I. Pakes, J. A. Garrido, and H. Kawarada, *MRS Bull.* **39**, 542 (2014).
- [2] F. Maier, M. Riedel, B. Mantel, J. Ristein, and L. Ley, *Phys. Rev. Lett.* **85**, 3472 (2000).
- [3] M. T. Edmonds, C. I. Pakes, and L. Ley, *Phys. Rev. B* **81**, 085314 (2010).
- [4] Y. Takahide, H. Okazaki, K. Deguchi, S. Uji, H. Takeya, Y. Takano, H. Tsuboi, and H. Kawarada, *Phys. Rev. B* **89**, 235304 (2014).
- [5] M. T. Edmonds, L. H. Willems van Beveren, O. Klochan, J. Cervenká, K. Ganesan, S. Praver, L. Ley, A. R. Hamilton, and C. I. Pakes, *Nano Lett.* **15**, 16 (2014).
- [6] G. Akhgar, O. Klochan, L. H. Willems van Beveren, M. T. Edmonds, F. Maier, B. J. Spencer, J. C. McCallum, L. Ley, A. R. Hamilton, and C. I. Pakes, *Nano Lett.* **16**, 3768 (2016).
- [7] F. Kueemeth, S. Ilani, D. Ralph, and P. McEuen, *Nature (London)* **452**, 448 (2008).
- [8] R. Winkler, S. Papadakis, E. De Poortere, and M. Shayegan, *Spin-Orbit Coupling in Two-Dimensional Electron and Hole Systems* (Springer, Berlin, 2003).
- [9] G. M. Minkov, A. V. Germanenko, O. E. Rut, A. Sherstobitov, L. E. Golub, B. N. Zvonkov, and M. Willander, *Phys. Rev. B* **70**, 155323 (2004).
- [10] G. Akhgar, D. L. Creedon, L. H. Willems van Beveren, A. Stacey, D. I. Hoxley, J. C. McCallum, L. Ley, A. R. Hamilton, and C. I. Pakes, *Appl. Phys. Lett.* **112**, 042102 (2018).
- [11] K. E. J. Goh, M. Y. Simmons, and A. R. Hamilton, *Phys. Rev. B* **77**, 235410 (2008).
- [12] See Supplemental Material at <http://link.aps.org/supplemental/10.1103/PhysRevB.99.035159> for the full details of the data correction and fitting, and the calculation of hole band dispersion and other parameters.
- [13] J. A. Garrido, T. Heimbeck, and M. Stutzmann, *Phys. Rev. B* **71**, 245310 (2005).
- [14] C. Nebel, C. Sauerer, F. Ertl, M. Stutzmann, C. Graeff, P. Bergonzo, O. A. Williams, and R. Jackman, *Appl. Phys. Lett.* **79**, 4541 (2001).
- [15] G. Bergmann, *Solid State Commun.* **42**, 815 (1982).
- [16] S. Hikami, A. I. Larkin, and Y. Nagaoka, *Prog. Theor. Phys.* **63**, 707 (1980).
- [17] W. Knap, C. Skierbiszewski, A. Zduniak, E. Litwin-Staszewska, D. Bertho, F. Kobbi, J. L. Robert, G. E. Pikus, F. G. Pikus, S. V. Iordanskii, V. Mosser, K. Zekentes, and Yu. B. Lyanda-Geller, *Phys. Rev. B* **53**, 3912 (1996).
- [18] A. Mal'shukov, K. A. Chao, and M. Willander, *Phys. Rev. B* **56**, 6436 (1997).
- [19] A. G. Mal'shukov, V. Shlyapin, and K. A. Chao, *Phys. Rev. B* **60**, R2161 (1999).
- [20] P. Mensz, R. Wheeler, C. Foxon, and J. Harris, *Appl. Phys. Lett.* **50**, 603 (1987).
- [21] P. M. Mensz and R. G. Wheeler, *Phys. Rev. B* **35**, 2844 (1987).
- [22] W. R. Anderson, D. Lombardi, R. Wheeler, T.-P. Ma, and P. Mitev, in Proceedings of Technical Papers, 1993 International Symposium on VLSI Technology, Systems, and Applications, 1993 (unpublished).
- [23] G. M. Minkov, O. E. Rut, A. V. Germanenko, A. A. Sherstobitov, B. N. Zvonkov, V. I. Shashkin, O. I. Khrykin, and D. O. Filatov, *Phys. Rev. B* **70**, 035304 (2004).
- [24] S. Cabañas, T. Schäpers, N. Thillosen, N. Kaluza, V. Guzenko, and H. Hardtdegen, *Phys. Rev. B* **75**, 195329 (2007).
- [25] H. Mathur and H. U. Baranger, *Phys. Rev. B* **64**, 235325 (2001).
- [26] T. Ando, A. B. Fowler, and F. Stern, *Rev. Mod. Phys.* **54**, 437 (1982).